Journal of Hydrology: Regional Studies 5 (2016) 293–308

Contents lists available at ScienceDirect

Journal of Hydrology: Regional Studies

journal homepage: www.elsevier.com/locate/ejrh

Extreme flood events in the Bolivian Amazon wetlands

A. Ovando[a,*], J. Tomasella[a], D.A. Rodriguez[a], J.M. Martinez[b], J.L. Siqueira-Junior[a], G.L.N. Pinto[a], P. Passy[c], P. Vauchel[b], L. Noriega[d], C. von Randow[a]

[a] Earth System Science Center (CCST), National Institute for Space Research (INPE), São José dos Campos SP, Brazil
[b] Institut de Recherche pour le Développement (IRD), France
[c] Department of Geography, National University of Singapore, Singapore
[d] Servicio Nacional de Meteorología e Hidrología (SENAMHI), Bolivia

ARTICLE INFO

Article history:
Received 23 June 2015
Received in revised form 6 October 2015
Accepted 10 November 2015
Available online 28 November 2015

Keywords:
Flood dynamics
Wetlands
Remote sensing
Llanos de Moxos

ABSTRACT

Study region: The Amazonian wetlands of Bolivia, known as the Llanos de Moxos, are believed to play a crucial role in regulating the upper Madeira hydrological cycle, the most important southern tributary of the Amazon River. Because the area is vast and sparsely populated, the hydrological functioning of the wetlands is poorly known.
Study focus: We analyzed the hydrometeorological configurations that led to the major floods of 2007, 2008 and 2014. These data, together with flood mapping derived from remote sensing images, were used to understand the dynamics of the Llanos during the three flood events.
New hydrological insights for the region: The results showed that large floods are the result of the superimposition of flood waves from major sub-basins of the region. As a previous study suggested, the dynamics of the floods are controlled by an exogenous process, created by the flood wave originating in the Andes piedmont that travels through the Mamoré River; and by an endogenous process, which is the runoff originating in the Llanos. Our study showed that the first process is evident only at the initial phase of the floods, and although important for attenuating the rising flood wave, it is of lesser importance compared to the endogenous process. We conclude that the endogenous process controls the magnitude and duration of major floods.

1. Introduction

Amazonian wetlands play a crucial role at the watershed scale because they are important habitats that support biodiversity of the ecosystem (Junk, 1997) and because they modulate water fluxes, both their quality and quantity. Amazon wetlands affect the basin sediment load, modifying water and dissolved and particulate material fluxes from upland watersheds through river drainage networks (Dunne et al., 1998; Guyot et al., 1996; Junk and Worbes, 1997; Meade et al., 1985; Melack and Forsberg, 2001; Mertes et al., 1996). Water residence time in wetlands alters river discharge due to the exchange of water between river and floodplain, and it promotes large evaporative losses (Bonnet et al., 2008; Mertes et al., 1995; Rudorff et al., 2014). In addition, water residence time in Amazon wetlands is crucial in the regulation of biogeochemical and biotic processes (Bouchez et al., 2012; Junk et al., 1989; Viers et al., 2005) and consequently carbon dioxide (CO_2) and

* Corresponding author. Tel.: +55 12 32087782.
E-mail addresses: alex.ovando@inpe.br, ovando.alex@gmail.com (A. Ovando).

http://dx.doi.org/10.1016/j.ejrh.2015.11.004

methane (CH_4) emissions (Abril et al., 2014; Kayranli et al., 2010; Melack et al., 2004; Richey et al., 2002). Both sediments and biogeochemical dynamics depend on the spatial and temporal patterns of hydrology, which, in addition to rainfall distribution, are also influenced by the topography, soil and vegetation (Mertes et al., 1995).

Over the period 2000–2014, the Amazon Basin has been affected by severe droughts (Espinoza et al., 2012; Marengo et al., 2008; Marengo et al., 2011; Tomasella et al., 2010) and floods (Marengo et al., 2012). The increased frequency of extremes in the Amazon has led Gloor et al. (2013) to suggest an intensification of the hydrological cycle starting from the 1990s, mainly concentrated in the wet season, which is responsible for "progressively greater differences in Amazon peak and minimum flows". It has been shown that these extreme events have the potential to cause serious disruptions in the ecological functioning of the "*terra firme*" Amazon forest ecosystems (e.g. Phillips et al., 2009) and alter the normal functioning of the wetlands, pushing the physiological adaptations and behavioral changes of living organisms beyond their resilience limits (Junk, 2013). In addition, they compromise the livelihoods of riverine communities, which are dependent on the flood pulses (Tomasella et al., 2013).

The Bolivian Amazon wetlands have also been affected by these extreme events. In terms of impacts and magnitude, the floods of 2007, 2008 and 2014 caused significant economic impacts and a large number of fatalities. According to CEPAL (2008), the floods of 2007 and 2008 caused losses of approximately $US 220 million in Bolivia, with approximately 250,000 affected people and 49 fatalities. The major flood of 2014 left 340,000 people affected, 64 fatalities, and 49,000 km^2 of crops lost. The losses in the livestock sector in the Beni Department reached $US 111 million with 350,000 people affected (Fundación-Milenio, 2014)

Sea surface temperature anomalies (SSTA) are believed to be influencing extreme flood events in the Bolivian Amazon (Ronchail et al., 2005; Ronchail et al., 2003). Higher than normal rainfall in the region has been related to a weak meridional sea surface temperature gradient (Ronchail et al., 2005). For this reason, the floods of 2007 and 2008 have been associated with El Niño and La Niña events, respectively (CEPAL, 2008), although the atmospheric processes associated with these extremes remain undocumented. The unprecedented rainfall over the Madeira Basin during the rainy season of 2013–2014, on the other hand, was related to warm conditions in the Pacific-Indian and sub-tropical south Atlantic, and exceptional warm conditions in the Atlantic Ocean, which favored the humidity transport over South western Amazonia (Espinoza et al., 2014). These features induced an anti-cyclonic anomaly over subtropical South America during January 2014, which enhanced rainfall over the Madeira Basin drainage area (Espinoza et al., 2014).

One of the major Amazonian wetlands is the "Llanos de Moxos", located between the Andes and the Brazilian shield, in the Southwest Amazon Basin within Bolivia. Like other wetlands in Amazonia, the "Llanos", because of its size and remoteness, is poorly monitored and therefore not well understood. To overcome this limitation, passive and active remote sensing techniques are crucial because they can provide information with the spatial and temporal resolution required in many studies. Passive systems have been used to characterize Amazonian wetlands in terms of vegetation, fluvial dynamics, limnology, geomorphology and flood extension despite their limitations due to interference from cloud coverage and vegetation (e.g. Alcantara et al., 2008; Arraut et al., 2013; de Lucia Lobo et al., 2012; Hamilton et al., 2002; Plotzki et al., 2012; Rudorff et al., 2009). Complementary, active systems (mainly Synthetic Aperture Radar—SAR) have proven to be extremely useful for mapping flood extension, vegetation, water stages and storage (e.g., Alsdorf et al., 2007; Arnesen et al., 2013; Hess et al., 2003; Martinez and Le Toan, 2007)

Moreover, remote sensing when combined with hydro-meteorological data makes it possible to understand the hydrological function of wetlands (Da Silva et al., 2010; Da Silva et al., 2012; Frappart et al., 2006). In this context, most of the existing knowledge of the flood dynamics in the "Llanos de Moxos" is based on the use of remote sensing and observational data (Bourrel et al., 2009; Hamilton et al., 2002; Hamilton et al., 2004) and more recently with the use of hydrological models (Paiva et al., 2013; Siqueira et al., 2015).

In this study, we have analyzed the hydrometeorological context of the 2007, 2008 and 2014 floods in the upper Madeira Basin and the dynamics of the Bolivian wetlands during those major floods events. We critically assess the temporal and spatial hydrological patterns that explain the magnitude and duration of those floods, both in the main rivers and wetlands. To achieve these goals, we have integrated hydrological and rainfall data from several sources in Bolivia, Brazil and Peru. Considering that the study region is vast and isolated, we complemented the scarce hydrometeorological data with multi-temporal flood maps based on the use of nouvelle remote sensing techniques. This study brings new insights to previous studies regarding the influences of extreme climatic conditions in the region, and it is a contribution to reducing the gap between common perception and scientific evidence regarding the floods in the region.

2. Wetlands of the Bolivian Amazon

The Bolivian wetlands, "Llanos de Moxos", is a vast savanna floodplain of approximately 150,000 km^2 (Hamilton et al., 2004) located in the Mamoré–Beni–Guaporé (Iténez) rivers fluvial system, between the eastern Andes, the adjacent Amazon alluvial fans and the Precambrian Brazilian shield (Fig. 1). The mean altitude at the "Llanos" is approximately 150 m with a mean slope less than 10 cm per km (Guyot, 1993). The natural vegetation is mixed: grassland and savannah vegetation in seasonally flooded areas, and evergreen tropical forests in non-flooded areas, although deforestation has converted part of the forest areas to pasture (Hamilton et al., 2004).

The hydrological dynamics of the "Llanos" is controlled by four major sub-basins (Fig. 1): the Guaporé (Iténez), the Mamoré, the Beni and the Madre de Dios, which define the upper Madeira River Basin, the main southern tributary of the

Amazon. Although the Madre de Dios River is outside the geographical region that delimits the "Llanos", the hydrological behavior of that river has a strong influence on the wetlands during major floods.

Altitudes in the four sub-basins range from 90 to 6500 meters above sea level (masl), where it is possible to differentiate three geomorphological regions: the lowlands (<800 masl), the Andean slope (800–3200 masl) and the high Andes (3200–6500 masl). The seasonality of precipitation in the Bolivian Amazon is governed by the South American Monsoon System (SAMS) composed of the Low Level Jet (LLJ), the Chaco low pressure system and the South Atlantic Convergence Zone (SACZ) (Marengo et al., 2004). SAMS determines the moisture transport from the Atlantic Ocean southwards through the Amazon during the rainy season (November to March), and it is estimated that 70% of the total annual precipitation occurs during these months (Navarro and Maldonado, 2004). Precipitation during dry months (June to September), if present, is generated mainly by cold frontal advections from the Antarctic anti-cyclone (Navarro and Maldonado, 2004). Incoming moisture from the Atlantic is deflected by the Andes, determining a particular spatial rainfall distribution across the Bolivian Amazon. The annual values in the lowlands vary southwards: from 2000 mm $year^{-1}$ in the northern part of the region to 1500 mm $year^{-1}$ in the central lowlands and 800 mm $year^{-1}$ in the southern part (Roche and Fernandez-Jauregui, 1988).

Rainfall variability westwards is highly influenced by the Andes: east-oriented Andean slopes capture moist warm air forming a humid belt (Espinoza Villar et al., 2009). In the piedmonts (<1500 masl), rainfall values range from 6000 mm $year^{-1}$ in the Mamore Basin, 4000 mm $year^{-1}$ in the Beni Basin, to 1700 mm $year^{-1}$ in the Mamoré (Roche and Fernandez-Jauregui, 1988). Rainfall decreases with altitude from 800 to 1000 mm $year^{-1}$ in the Andean summits of the Beni and Madre de Dios basins (>4500 masl) to 450 mm $year^{-1}$ in the upper Mamoré basin (~2500 masl) (Roche and Fernandez-Jauregui, 1988).

The strong contrast between dry and rainy season leads to annual variability in discharge. In the Andes and piedmonts, hydrographs have multiple peaks and lows, denoting a rapid response to rainfall. Downstream, the hydrograph is smoothed and floods occur generally during summer (Roche and Fernandez-Jauregui, 1988; Ronchail et al., 2003; Ronchail et al., 2005). Interannual variability in streamflow may influence flood intensity and extension depending on the meteorological conditions in the Andean slopes-piedmonts and within the lowlands (Espinoza Villar et al., 2009; Roche et al., 1992). Thus, variable sources of floodwaters that include distinct upland watersheds and local precipitation result in high variability in both the magnitude of the flooding and droughts (Hamilton et al., 2004; Hanagarth, 1993).

3. Methods

3.1. Data

3.1.1. Hydrometeorological data

We used hydrometeorological data from different sources in Bolivia, Brazil and Peru. Rainfall data integrated information from the Brazilian National Institute of Meteorology (INMET), the Brazilian National Institute for Space Research

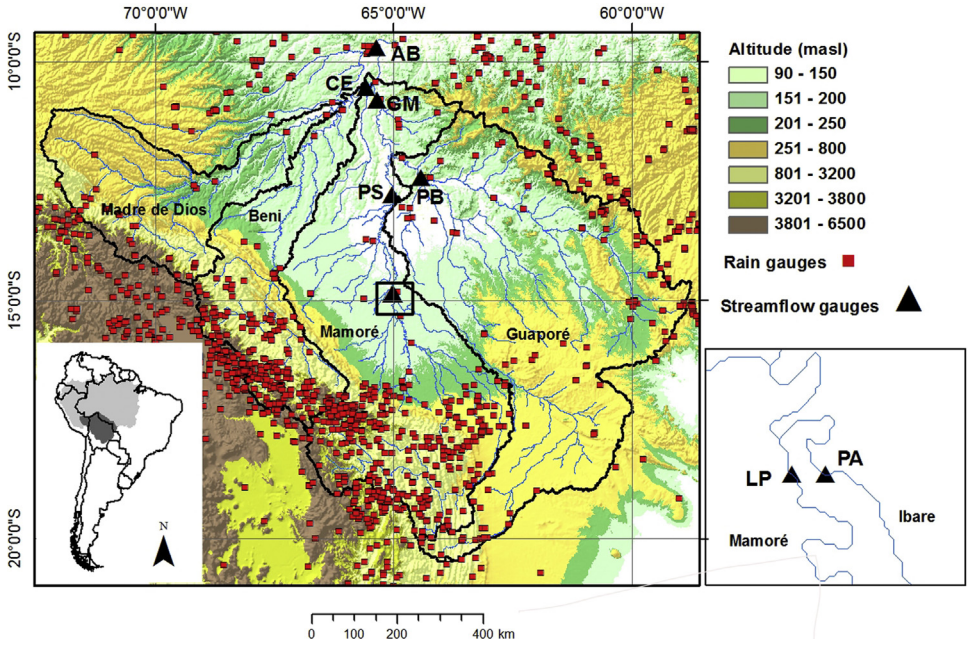

Fig. 1. The upper Madeira Basin in Bolivia. Major sub-basins are delimited by black polygons; the red dots represent rain gauge locations; black triangles indicate the following gauge stations: Abunã—AB, Cachuela Esperanza—CE, Guajará-Mirim—GM, Príncipe da Beira—PB, Puerto Siles—PS, Puerto Almacén—PA and Los Puentes—LP (see right inset for detailed location). (For interpretation of the references to color in this figure legend, the reader is referred to the web version of this article.)

Table 1
List of stations used to characterize the hydrological behavior of the Llanos.

Code	Station	Longitude	Latitude	River	Drainage area (km^2)	Mean discharge 1984–2014 ($m^3\ s^{-1}$)
PS	Puerto Siles	−65.03	−12.78	Mamoré	230047	4157.00
PB	Príncipe da Beira	−64.42	−12.43	Guaporé (Iténez)	341000	2233.10
CE	Cachuela Esperanza	−65.57	−10.54	Beni/Madre de Dios	281000	8074.00
GM	Guajará-Mirim	−65.35	−10.79	Mamoré/Guaporé	609000	7247.60
AB	Abunã	−65.36	−9.70	Madeira	921000	15857.06
LP	Los Puentes	−65.04	−14.88	Mamoré	153000	–
PA	Puerto Almacén	−65.01	−14.88	Ibaré	5864	–

(INPE) and discharge and water level data from the Brazilian Water Agency (ANA). Rainfall data from Bolivia and Peru were respectively extracted from the Bolivian and Peruvian Meteorology and Hydrology National Service—SENAMHI-BO and SENHAMI-PE. Hydrological data was made available by the Project "Geodynamical, hydrological and biogeochemical control of erosion/alteration and material transport in the Amazon basin"—SO HYBAM, which network is operated with SENAMHI-BO and SENHAMI-PE. Rainfall data were analyzed in order to detect inconsistencies, according to the methodology suggested by the Brazilian Water Agency (ANA, 2012). Then, raingauge data were interpolated to the whole catchment using the method proposed by Lefevre et al. (2002), which is based in the inverse of the squared distance weighted by the station altitude. This is necessary considering that basin rainfall is strongly affected by orographic effects (Espinoza Villar et al., 2009). These data were qualified for analyzing the temporal and spatial distribution of rainfall anomalies over the study region using the climatology for the period 1970–1990 derived by (Siqueira-Júnior et al., 2015).

The dynamics of the "Llanos" was analyzed using data from the stations listed in Table 1. The Abunã gauging station is located downstream from the confluence of the Beni, Abunã and Mamoré Rivers (Fig. 1), which join to form the Madeira River. The Beni River rises in the hillslopes of the Bolivian Andes northward, and it receives the discharge from the Madre de Dios River, which rises in the Peruvian Andes and flows eastward. The discharge at the Cachuela Esperanza gauge station, located downstream of this confluence, indicates the contribution of the northwestern part of the study area. The Mamoré River born in the Bolivian Andes, to the south of the study area, drains the precipitation falling over the western part of the basin and flows toward the north through the "Llanos", where the Puerto Siles gauge station is located, to finally meet the Guaporé (Iténez) river at the Bolivian-Brazilian border. The Guaporé River drains the southeastern part of the study area, receiving the contribution of several streams from Bolivia and Brazil, including the semi endorheic Parapeti basin. Upstream of the confluence of the Guaporé with the Mamoré, the Principe da Beira gauging station is located, whereas downstream of this confluence, the representative gauge station is Guajará-Mirim.

Finally, exchange between the wetlands floodplain and the Mamoré main-stem was analyzed using water stage data from the stations of Los Puentes, located in the Mamoré River, and Puerto Almacén, which records data from the Ibare River, a tributary of the Mamoré in the Llanos area. Both stations are operated by the Service for the Improvement of Amazon Navigation – SEMENA – Bolivia.

Because the onset of the wet season in the study area is between mid-October and mid-November, the floods of 2007, 2008 and 2014 were respectively described for the following periods: October 2006–September 2007, October 2007–September 2008 and October 2013–September 2014.

3.1.2. Remote sensing data

Multi-temporal maps of flooded area for the floods of 2007, 2008 and 2014 were derived using both active and optical systems: MODIS (Moderate Resolution Imaging Spectroradiometer) and PALSAR (Phased Array Synthetic Aperture Radar). MODIS data include seven spectral bands in the 400–2500 nm spectral region at 500 m spatial resolution (http://modis.gsfc.nasa.gov). The near infrared (NIR—841–576 nm) and middle infrared (MIR—1230–1250 nm) channels make it possible to capture the variation of the floodplain surface during the hydrological cycle as a function of vegetation growth, water availability and flooding. We used the MODIS MOD09A1 surface reflectance 8-day composite product because it provides the best available pixel in an 8-day period, reducing the amount of data to analyze and the effects of gaseous absorption, aerosol scattering and other atmospheric artifacts. Terra and Aqua MODIS M*D09A1 images for the slot 01/01/2001–09/09/2014 were collected from public repositories (https://lpdaac.usgs.gov/), resulting in 2248 images.

PALSAR is an active L-band sensor aboard the Land Observation Satellite (ALOS) launched in 2006 by the Japanese National Space Agency (JAXA). PALSAR data make it possible to detect water under vegetation canopy due to the L band double bounce effect with relative independence from atmospheric conditions (Woodhouse, 2006). Forty-five PALSAR. L1.5 product, ScanSar HH images were selected to cover most of the floodable areas in the Bolivian Amazon while capturing different flood stages (dry, wet and intermediate) and to have homogeneous coverage in terms of acquisition dates. Thus, six mosaics from March 2007 to March 2009 were generated.

3.2. Flood mapping

3.2.1. Image pre-treatment

ALOS PALSAR Product L1.5 images already includes corrections of range spreading loss, antenna pattern and incidence angle corrections. Thus, previous image treatment included data transformation-correction, registration, mosaicking and

filtering. Image transformation is the process of converting a linear amplitude image into a radiometrically calibrated power image. Then, the original digital numbers (original pixel values—DN) were transformed into sigma values (σ^0), which is the ratio of the incoming and backing power in a patch of ground.

$$\sigma_0 = a_2 \left(\mathrm{DN}^2 - a_1 N_r\right) \tag{1}$$

where N_r is the noise offset and a_1 and a_2 are scale and linear conversion factors determined during the calibration of the processor. To analyze the backscatter response for different land cover units, the values resulting from Eq. (1) were converted into dB values using the following equation:

$$\mathrm{d}B = 10 \times \log_{10}(\sigma_0) \tag{2}$$

Mosaics covering the study area were assembled for every date, and then, once coregistered, multitemporal and spatial speckle reduction filters were applied. To increase the equivalent number of looks (ENL) by exploiting the temporal information available in the time series for each pixel, we applied a multitemporal filter developed by (Quegan et al., 2000). For a sequence of N registered multitemporal images with intensity at position (x, y) in the kth image denoted by $I_k(x, y)$, the temporal filtered images are given by:

$$j_k(x, y) = \frac{E[I_k]}{N} \sum_{i=1}^{N} \frac{I_i(x, y)}{E[I_i]} \tag{3}$$

$k = 1, \ldots N$, where $E[I]$ is the local mean value of pixels in a window centered at (x, y) in image I.

This filter makes possible to improve ENL and at the same time to preserve spatial resolution. Additionnal conventionnal filtering is classicaly aplied to further improve the ENL in order to achieve appropriate radiometric stability (Martinez and Le Toan, 2007).

Image treatment and analysis of MODIS images followed these steps: (i) cloud masking, using ancillary pixel information provided by the MODIS-MOD09A1 product; (ii) selection and delineation of sampling areas—AOI considering a variety of land cover units along the study area; (iii) reflectance analysis for each of the selected AOI by automated procedures; and (iv) development of classification criteria using key values and thresholds of infrared bands.

Spectral analysis of MODIS reflectance and PALSAR backscater signatures provided key information regarding its temporal variation along the floodplanis, details can be found in Supplement S1.

3.2.2. *Image classification*

Classification was based on an object-based image analysis (OBIA) approach (Blaschke, 2010), using segments or clusters-based mapping algorithms rather than pixel-based schemes. Image. Segmentation was achieved by exploring spatial connectivity and spectral similarity between pixels in order to form groups of homogeneous pixels. The statistical mean was computed at the cluster level and then used in the flood mapping algorithm. Spatial segmentation was performed in the PALSAR image dataset since it present the finest spatial resolution, and was subsequently applied on the MODIS images that were registered to the same geometry. This procedure generated smoother maps without excessive outlier pixels, and, in the case of the MODIS images, it tackled the lack of information resulting from extensive cloud cover in most of the wet season images. We applied the eCognition software (Trimble, 2011) to perform the segmentation, using the Multiresolution segmentation method, giving all the layers the same weight, and assigning weights of 0.4 and 0.8 to shape and color (compactness) parameters, respectively.

Classification algorithms and data analysis for both the ALOS-PALSAR and MODIS systems were performed based on their respective backscatter and reflectance temporal variation. Temporal changes between dry and wet seasons are related directly to the progression of flooding. Initially, by using the dry season signals and total change estimations, different land cover types are defined; then, the signal change between dry and wet season is used as a flood indicator.

For PALSAR images, the temporal variation across the time series is estimated by an Absolute Change (AC) estimator algorithm (Quegan and Le Toan, 1998). It estimates the logarithm of the ratio between any date within the multi-date data set (Quegan et al., 2000) according to Eqs. (4) and (5).

$$\mathrm{AC} = 10\log\lfloor \frac{2}{2N-1} \Sigma_{i=1}^{N} \Sigma_{ji} R_{ij} \rfloor \tag{4}$$

$$\text{with} \quad R_{ij} = \max\left(\frac{i}{j}, \frac{j}{i}\right) \tag{5}$$

The AC computes the total unsigned backscatter change using the maximum ratios for every possible image couple. Then, the ratios are summed and normalized by the number of images. The AC provides positive values in decibels, which in combination with dry season radar signals and dry season MODIS NDVI values, allows to obtain a land cover map with four classes: water bodies, dense forests, sparse forests, and savannas; and three flood susceptibility subclasses: floodable dense forest, floodable sparse forests and floodable savannas. (Details in Supplementary material S1). The accuracy of this map was validated with a wetland extent map generated from JERS-1 SAR data (Hess et al., 2015b), in which wetlands were defined as the inundated areas during radar acquisition dates (October–November 1995 or May–July 1996), or adjacent areas

displaying landforms consistent with wetland geomorphology (Hess et al., 2015a). Details of the validation are provided in Supplementary material S3. The flood status for every land unit is determined by contrasting backscatter from every image with a referential dry season image, leading to a more complex class definition. If the backscatter signal changes until a fixed threshold, then the unit is classified as saturated or flooded. Submerged areas present a dramatic backscatter decrease, while saturated zones show increasing return as a function of vegetation structure. This second step gives birth to a more complex class definition that splits each vegetation class in either flooded/non-flooded sub-class.

The classification of optical images is based on the radar image typology in terms of spatial clustering and vegetation type. Thresholding the MIR and NIR channels allows one to discriminate flood status classes, also with a more complex class definition (Supplementary material S2).

We evaluated the robustness of the flood mapping based on the MODIS time series by comparing the resulting areas estimates with the areas assessed from an independent dataset. To achieve this objective, we analyzed PALSAR L-band SAR times series in order to compare the flooded savannas area and the flooded forested area estimates for five different flood stages including rising flood (December 2007), flood peak (March 2007, March 2008, March 2009) and decreasing flood (June 2007). As L-band microwave is known to penetrate deeply the vegetation cover and the PALSAR images stand as the best dataset allowing for a reliable estimates of the flooded area under forest cover. Comparison between SAR data and MODIS data is not straightforward as there is no SAR sensors acquiring images with the same time frequency and spatial resolution than MODIS. Furthermore, visible and infrared light and radar microwave do not interact the same way with the vegetation, the soils and the water surface. In this way, we do not expect both SAR and MODIS flood estimates to match perfectly but we assume that their comparison is a fair assessment of the robustness of MODIS-derived flood maps (Supplementary material S3).

4. Results and discussion

4.1. Hydrological regime of the upper Madeira Basin

In addition to the contrasting differences in seasonal discharge of the sub-basins of the upper Madeira River due to differences in climate regime, the hydrological response is quite distinctive mainly because of the topographic characteristics of the middle and lower drainage areas. Because the Madre de Dios River has steeper topography and smaller contribution area compared with the other sub-basins, its hydrological response is faster and characterized by spiky behavior, and it has a strong influence on the peak and shape of the flood waves of the Beni River. The Mamoré River, on the other hand, flows along the vast "Llanos" wetlands, which reduces the peaks and significantly delays the travel time of the flood waves coming from the Andes. This explains why the peak discharge at Cachuela Esperanza station in the Madre de Dios-Beni River system occurs, on average, 54 days before the peak in Guajará-Mirim station in the Mamoré–Guaporé river system.

In the Madeira River, at the Abunã station, peak discharges occurs, on average, 8 days after Cachuela Esperanza and 46 days before the peak in the Mamoré–Guaporé river system. The time difference between the peaks of the Madre de Dios-Beni river system, coming from the west part of the study area, and the Mamoré–Guaporé River system, coming from the east, attenuates the discharge of the upper Madeira and prevent the occurrence of extremely high river levels at Abunã station.

4.1.1. Hydrometeorological context of the 2007, 2008 and 2014 flood events in the upper Madeira Basin

Flood events are reported periodically in the Llanos because this area is naturally exposed and dependent on regular annual flood pulses. However, the extreme characteristics of the 2007, 2008 and 2014 flood events created serious concerns in local communities not only because of their magnitude but most importantly because they were concentrated in less than a decade. Although the floods of 2007 and 2008 should be classified in the above-normal category, we consider the three events as "extreme" since floods of the same magnitude than that of 2007 (+27% from mean flood peak for the period 2001–2014) resulted in strong impacts on the economy of local communities and triggered several civil protection actions (CEPAL, 2008). To analyze these extreme events, Fig. 2a and b shows rainfall anomalies in the study area for the wet season periods associated with the three events, that is, October 2006–March 2007, October 2007–March 2008 and October 2013–March 2014. In addition, Fig. 3 shows daily discharges during 2007, 2008 and 2014 against the long-term mean discharges of the period 1984–2014.

4.1.1.1. The flood of 2007. Rainfall during the rainy season of 2007 was higher than the climatological average mainly over the drainage areas of the Mamoré and Guaporé rivers. Major rainfalls occurred over the headwaters of these basins in January 2007 and over Beni and Madre de Dios basins in February 2007 (Fig. 2b). These positive rainfall anomalies were responsible for higher than average discharges at Guajará Mirim station from late February through middle June and from early March to middle June in Puerto Siles gauge stations. At Principe da Beira, discharge was also above the mean from the beginning of the rainy season (October) until June. Although the Mamoré River peaked 16 days later than expected from the long-term average in Puerto Siles, the peak in Guajará Mirim occurred only 3 days earlier than the average time. The delay in the time of the peak that occurred in the Mamoré River in Puerto Siles station reduced the lag time between the peaks of the Mamoré and Guajará Mirim rivers (Fig. 3), almost superimposing the peaks of the flood waves of the two rivers at Guajará Mirim station, exacerbating the discharge levels close to the peak.

At the Beni River at Cachuela Esperanza station, higher than average discharges were observed from late February though early June, and the peak discharge was delayed 14 days from the expected average. This delay in the peak reduced the normal time-delay between the contribution of the western and eastern portions of the upper Madeira Basin, and also delayed the peak of the Madeira River at Abunã station. The fact that the contributions of both parts of the basin were "almost in phase" explains the exceptional discharges observed during the 2007 flood.

4.1.1.2. The flood of 2008. During the hydrologic year of 2007–2008, discharges higher than average were observed in Guajará Mirim from December through June due to above average rainfall occurring over the Mamoré–Guaporé basin during the rainy season (Fig. 2a and b). The largest positive anomalies of precipitation were observed in January 2008 over the basin.

Although discharge data during the peak of the hydrograph in Principe da Beira are missing, a visual analysis of Fig. 3 indicates that this peak occurred during the first half of May, later than expected. Discharges were above the long-term average from February 2008 until September 2008. Exceptionally higher than long-term average discharge was also recorded in the Mamoré River at Puerto Siles from December through May, and the peak timing was slightly delayed from the average. Due to the severity of the 2008 flood at the Mamoré River, the discharge at Guajará Mirim was well above the long-term average, and the peak occurred 17 days earlier than average, in middle April 2008. The reason for the water stage behavior at Guayará Mirim during 2008 is related to the spatial distribution of rainfall: a large amount of rainfall accumulated during February and March over the lower part of the Mamore basin, downstream of Puerto Siles (Fig. 2a and b). This anomalous

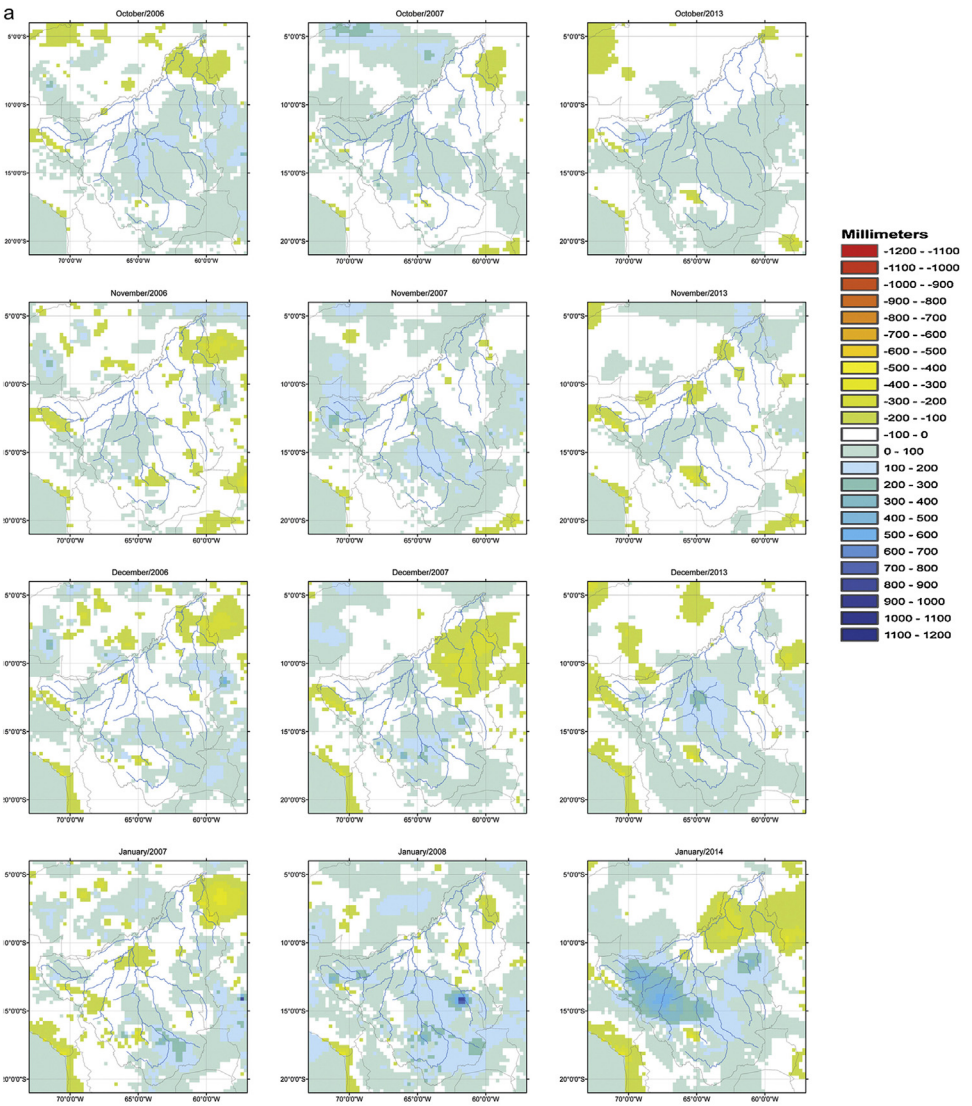

Fig. 2. (a)Monthly rainfall anomalies from October 2006 to January 2007 (left column); October 2007 to January 2008; and October 2013 to January 2014. (b) Monthly rainfall anomalies from February 2007 to April 2007 (left column); February 2008 to April 2008; and February 2014 to April 2014.

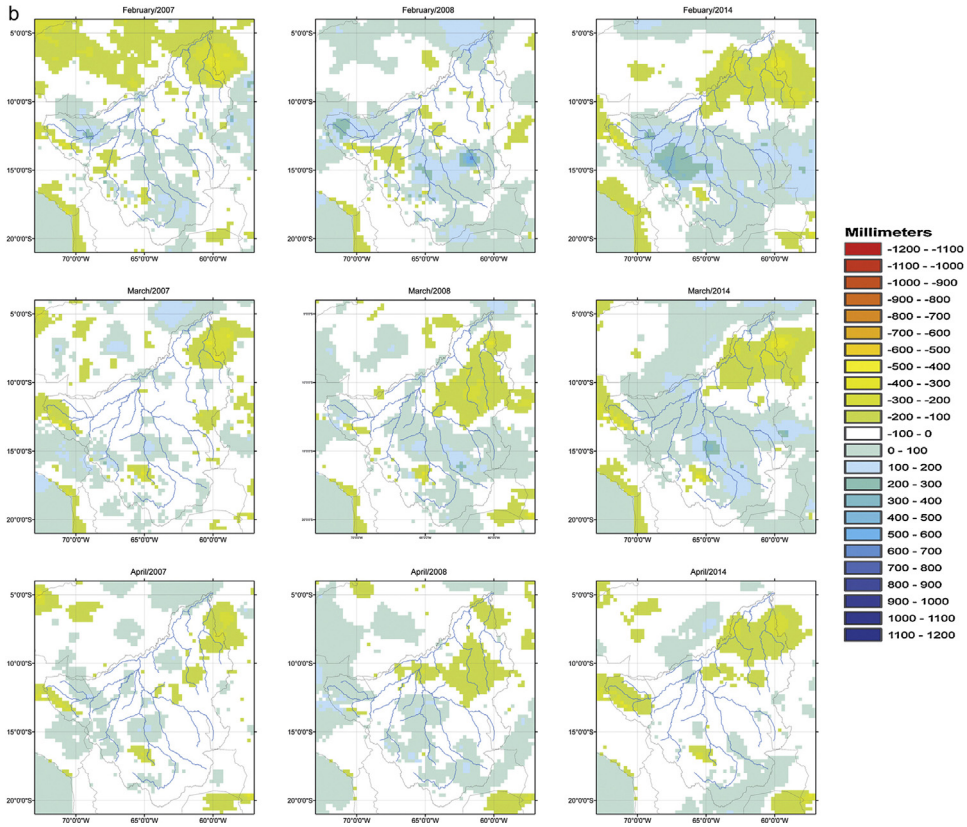

Fig. 2. (*Continued*).

rainfall located close to Guayará Mirim station suffered almost no attenuation, and it added to the crest of the flood coming upstream from the Mamoré River, resulting in the exceptional discharges observed at Guajará Mirim station (Fig. 3).

In Cachuela Esperanza, the Beni River discharges were higher than the long-term average from October through April, and the maximum discharge was recorded 23 days before the long-term average. However, a secondary peak occurred in early April (09/04), directly associated with the positive rainfall anomalies in the headwaters of the Madre de Dios sub-basin

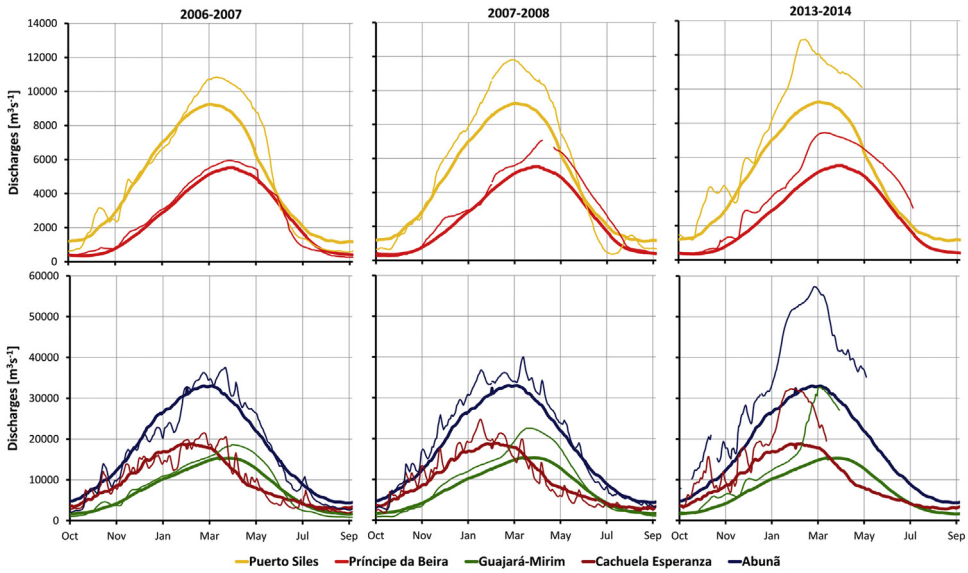

Fig. 3. Hydrograph of the mean monthly discharge (thick lines) during the 2007, 2008 and 2014 flood events (thin lines) for different discharge stations.

(Fig. 2a and b). This second peak almost coincided with the higher discharges recorded at Guajará Mirim station. This second late peak, a few days before the peak at Guajará Mirim, drove water levels in the Madeira River to exceptionally high values at Abunã station. Moreover, Abunã registered discharges higher than the average from the beginning of the rainy season (October) until early June, and the peak was observed 25 days later than expected from the long-term average.

4.1.1.3. The flood of 2014. Rainfall above the climatological mean was observed in December 2013 over the confluence area of the Guaporé and Mamoré rivers. Later, positive rainfall anomalies spread over the whole upper Madeira basin, with the largest values over the drainages areas of the Beni-Madre de Dios River system during January 2014 (Fig. 2a and b).

This anomalous rainfall produced exceptionally higher than normal discharge in the Mamoré River at Puerto Siles in February 2014 and in the Guaporé River at Príncipe da Beira in March 2014. In Puerto Siles, the peak was observed only 9 days before the long-term average, whereas in Príncipe da Beira, it was 22 days earlier than average. The peak time at Puerto Siles matched the beginning of an abrupt increase of discharge at Guajará-Mirim during the first days of March. Discharge above the average was recorded in Guajará Mirim from the beginning of the rainy season (October), and the hydrograph peak occurred by the end of March, one month earlier than expected from the long-term hydrograph. The river Beni at Cachuela Esperanza showed discharges exceptionally higher than the long-term average since October 2013. During Mid-January, discharge increased abruptly in response to abundant rainfall in the Beni and Madre de Dios contributed areas. The peak at Cachuela Esperanza station was recorded 14 days earlier than expected from the long-term averaged hydrograph (Fig. 3).

By the time that the flood wave coming from the Mamoré–Guaporé river system had reached its peak at the Guajará-Mirim station, discharge in the Madeira River at Abunã station was well above the long-term average because it was receiving significant flows from the Beni-Madre de Dios River System. Moreover, during 2014, both the Beni-Madre de Dios and Mamoré–Guaporé river systems showed exceptionally high discharges, and both systems peaked at the Madeira confluence almost simultaneously, superimposing the flood waves of the eastern and western upper Madeira Basin. In addition to the fact that the flood waves coming from different areas of the basin were in phase, the flood of the Madeira River at Abunã was exacerbated by intense local rainfall at peak time.

4.2. Flood dynamics in the Llanos during the 2007, 2008 and 2014 events

4.2.1. Spatial and temporal variability of floods

The multi-temporal series of flood maps obtained from MODIS images for the time slot 2001–2014 allowed to identify the peculiar characteristics of the Llanos de Moxos. Flood peaks tend to occur between March and April, whereas during August–September, floods are primarily related to permanent water bodies (lakes and rivers). A conspicuous degree of interannual variability is observed, with a range of 50,293 km^2 between the maximum flood peak (2014) and the minimum flood peak (2012). The average flood peak reaches 36,859 km^2 with a standard deviation of approximately 14,357 km^2 (Fig. 4). These metrics clearly show that there is a complex dynamic in terms of flood extension and timing.

When comparing these results with those obtained by Hamilton et al. (2004), who performed flood estimations for the period 1978–1987 from passive microwave radiometry, it is possible to note both similarities and disparities. Our estimation indicate that permanent open water are approximately 3700 km^2 against 4780 km^2 estimated by Hamilton et al. (2004). The annual flood cycles are similar (peaks in March–April and minimum in August–September); the maximum flood extension estimated in this study, including permanent water bodies, was 71,305 km^2, approximately 12,000 km^2 less than Hamilton's estimation for 1982 (83,248 km^2). The medium values of inundation including permanent open water for the period 1979–1987 derived by Hamilton et al. (2004) was 28,163 km^2, against 9835 km^2 for the period 2001–2014. These differences are partly related to the different remote sensing techniques employed, as well as differences in the hydrological regime of the two periods considered as suggested by statistical tests in the hydrological station in Puerto Velho, which is the only station who has available data for the period 1979–2014. The non-parametric Wilcoxon and Kolmogorov tests rejected, with 5% of confidence, the null hypothesis of equal medians and equal distributions, respectively, between the discharges in Porto Velho between the periods 1979–1987 and 2001–2014. Also, the Pettit test for homogeneity applied to the 1979–2014 series rejects the null hypothesis at the same level of confidence.

In addition, making use of visual interpretation of optical and SAR high resolution images (pixel of about 30-m size), Bourrel et al. (2009) assessed a flooded area of 30,000 km^2 for the 1997 flood. Other maximum flood estimations in the area, such as 150,000 km^2 reported by Junk (1993), 100,000 km^2 estimated by Hanagarth (1993) or 215,171 km^2 estimated by Crespo and Van Damme (2011), are based on floristic and vegetation composition rather than on water detection from remote sensing techniques, and they are not reported in yearly time steps. Hence, no direct comparisons were performed with them.

It is possible to distinguish that the events of 2007, 2008 and 2014 are the most representative of the period 2001–2014 in terms of magnitude and behavior (Figs 4 and 5). The maximum flooded area was 40,676 km^2 on 22/03/2007, exceeding by +27% the mean flood peak for the 2001–2014 period; 59,694 km^2 on 07/04/2008, exceeding by +62%; and 71,305 km^2 on 06/03/2014, with +93% above the mean.

Fig. 6a and b show the flood dynamics of the Llanos areas for the 2007, 2008 and 2014 events for different dates, shown as vertical bars in Fig. 5: continuous bars indicate that the flooded area is increasing, whereas dotted vertical bars correspond to when the water is receding in the floodplain.

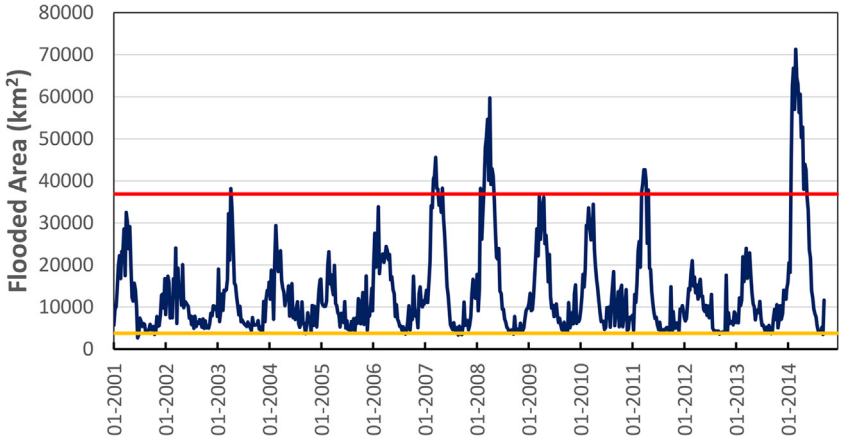

Fig. 4. Time-variation of the flooded area in the study area during period 2001–2014. The horizontal red line indicates the mean of the flood peaks; the yellow solid line indicates the minimum open water extension. (For interpretation of the references to color in this figure legend, the reader is referred to the web version of this article.)

Fig. 6a shows that the flooding begins in isolated spots in the central area of the Llanos, in endogenous streams, rivers and lakes, suggesting the existence of a threshold storage level in several small lakes that needs to be reached to allow exchange with the drainage network. It is noticeable, in the case of the 2007 and 2008 floods, the displacement and expansion of the flooded area from the southern part to the center of the Llanos, close to Puerto Siles station, a process that occurred along the Mamoré main-stem simultaneously with the movement of the river flood-wave. When this gradually growing flooded area reached the center of the Llanos, the flooding generalized to the whole area of the wetlands. This process was not as evident during the 2014 flood, presumably because the magnitude of the rainfall and consequently the dynamics of the process were so fast that the temporal resolution of the images could not capture that behavior.

It is also clear that there were differences in the timing of the three events: although in the 2007 flood event, the increase in the flooded area became evident by the beginning of March, during the 2008 and 2014 events, the flooded area was noticeable already in early February, particularly during 2014. This is related to the fact that in the event of 2007, positive rainfall anomalies were observed in January 2007, whereas in the floods of 2008 and 2014, above-the-mean rainfall was observed from November 2007 and December 2013, respectively (Fig. 2a and b).

The flooded area in February in the western part of the "Llanos" was much larger in 2014 compared to 2008. However, in the eastern part, particularly between late March and during April, the situation was the opposite (Fig. 6a and b); thus, the eastern flooded area was larger in 2008 compared to 2014. This illustrates the effect of local rainfall on the dynamics of the wetlands: in January and February 2008, the eastern portion of the Mamoré contribution area was affected by intense localized positive rainfall anomalies. Although in January and February 2014 positive rainfall anomalies were spread over the Mamoré contribution area, very intense rainfall spots were located in the upper Mamoré only in 2008 (Fig. 2a and b).

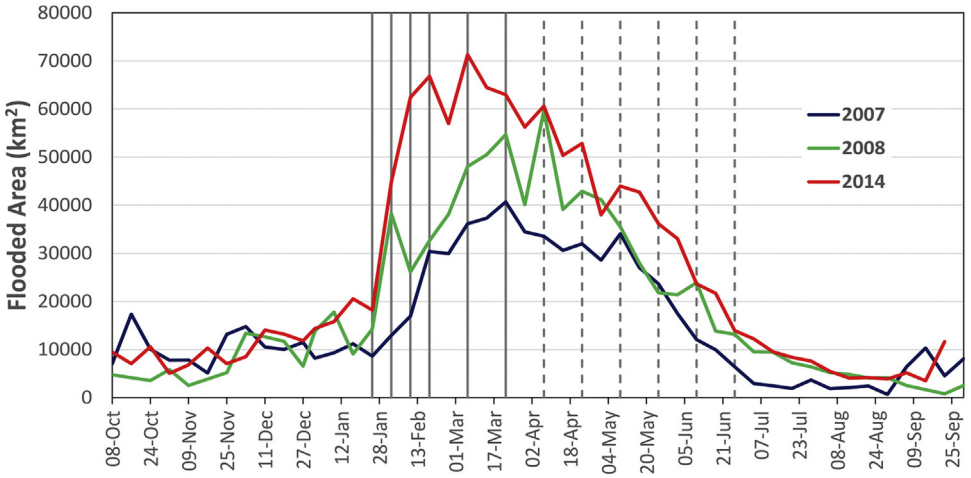

Fig. 5. Time-variation of the flooded area during the 2007, 2008 and 2014 flood events. Vertical lines indicate the dates of the flood maps of Fig. 6a and b.

On the other hand, during 2014, the strongest positive rainfall anomalies persisted in the upper Madre de Dios-Beni river system during January and February 2014 (Fig. 2a), explaining why the flood was extended to the west in 2014 compared to 2008. Therefore, localized rainfall is a determinant of the dynamics of a flooded area.

Time variation in the three flood events was also verified during the recession of the flooded area: Fig. 5 indicates that during the 2007 event, the Llanos had returned to its initial condition of January by June 10th, while in the other two events the flooded area was still evident. This is related to the fact that rainfall returned to normal by March 2007, whereas in 2008 and 2014 rainfall higher than the climatological mean persisted over the Beni and Mamoré basins. Therefore, the extension of the flooded area depends not only on the magnitude of rainfall anomalies but is also directly related to the time-persistence of positive rainfall anomalies. Although March marks the end of the wet season and the rainfall amounts

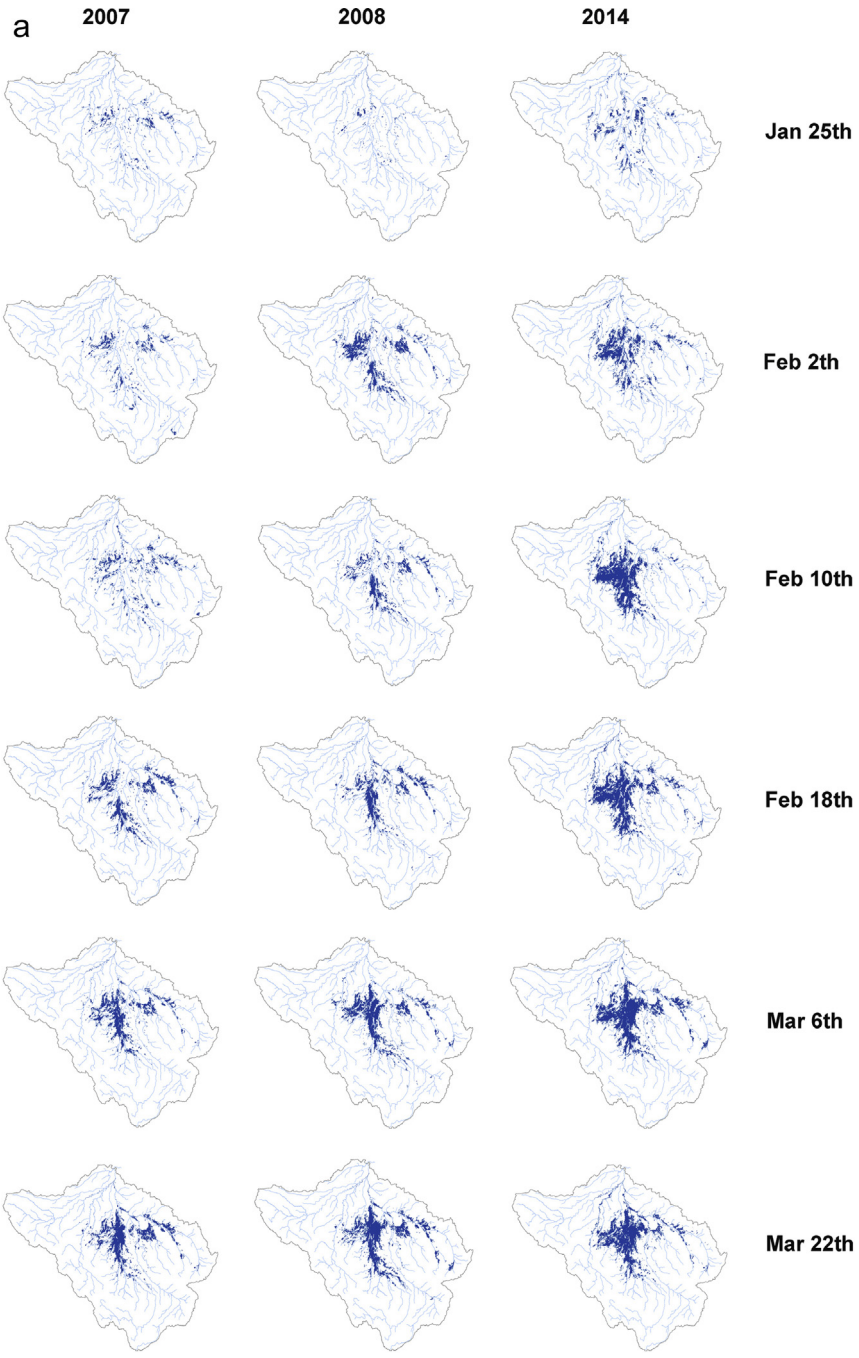

Fig. 6. (a) Flood dynamics of the Llanos areas for the 2007, 2008 and 2014 events from January to March. (b) Flood dynamics of the Llanos areas for the 2007, 2008 and 2014 events from April to June.

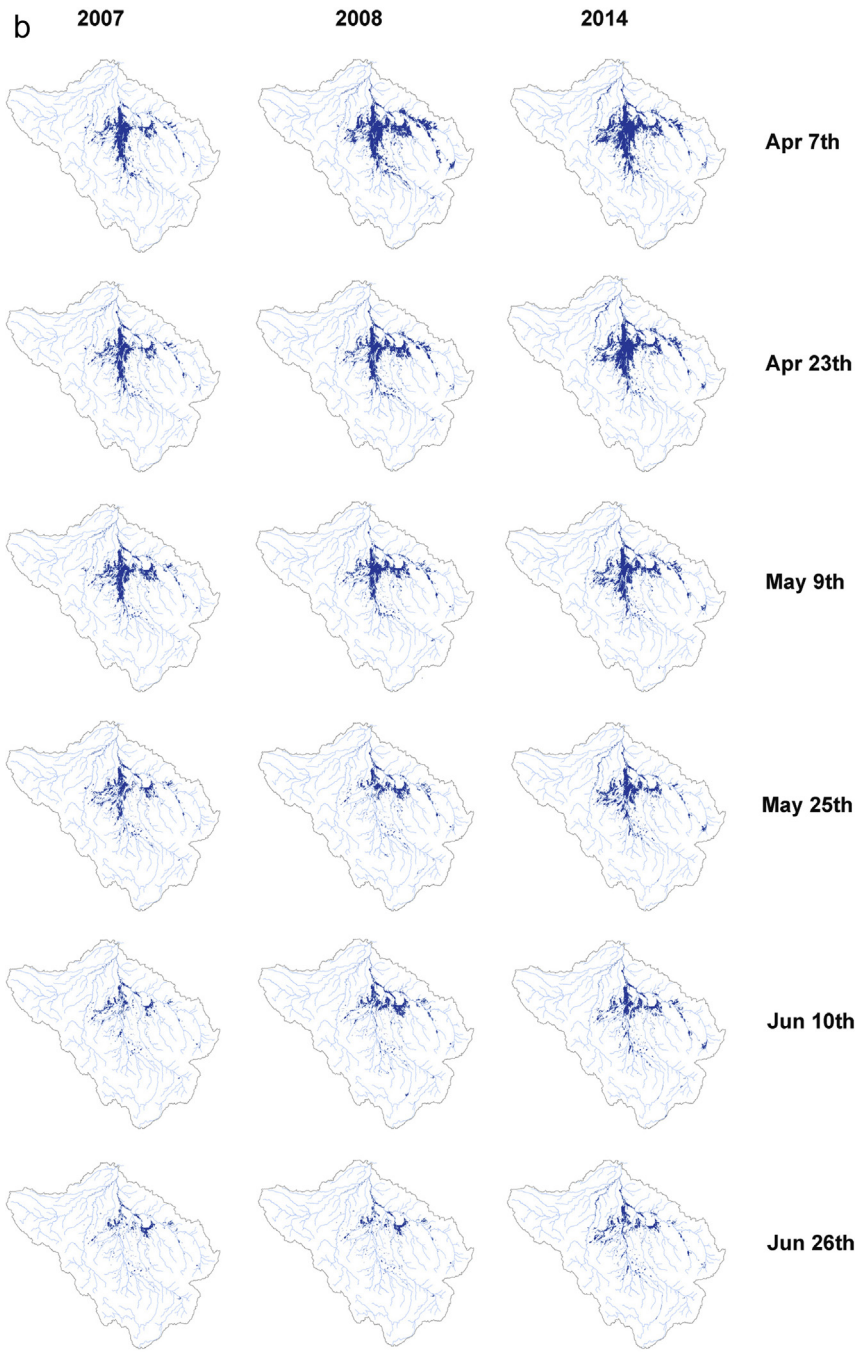

Fig. 6. (*Continued*).

are already declining, above normal values during this month have the potential to cause significant surface runoff because the flooded area is usually close to its maximum.

Fig. 7 shows the relationship between flooded area and the stage at Puerto Siles gauge station. Although there is a clear relationship between the flooded area and the gauging station, a loop in the relationship is also evident with the river's rise and recession observed in the three floods. This behavior is explained by the arrival of the flood pulse coming through the Mamoré River, shown in Fig. 6a: the flooded area gradually increases upstream of Puerto Siles station before the gauge can detect significant variation of the water stage. However, at the peak time of Puerto Siles, the flooded area reaches its maximum, indicating that the station is a good proxy for the flooded area of the wetlands. Moreover, during the recession, the relationship is stable and well defined regardless of the previous history of the flood event.

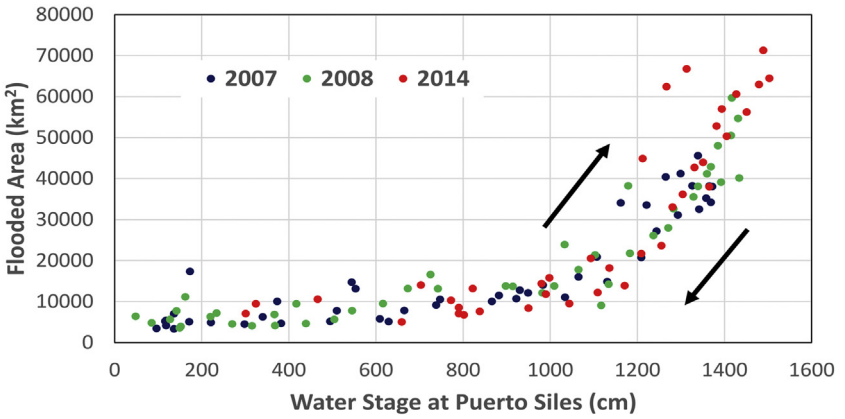

Fig. 7. Relationship between flooded area and water stage at Puerto Siles during the three floods. Arrows indicate the time evolution of the floods.

4.3. *Hydrological functioning of the Llanos*

Bourrel et al. (2009) hypothesized that the floods in the Llanos are controlled by two different processes:

- An exogenous process resulting from the arrival of the flood wave from the Mamoré River and other tributaries generated in the Andes piedmont;
- An endogenous process resulting from the outflow of water from the wetlands in response to local precipitation, which can be temporarily blocked by high water levels of the exogenous flood wave at the Mamoré main-stem.

Bourrel et al. (2009) suggested that wetlands dynamics vary markedly from year to year: sometimes, the endogenous process controls almost the entire flood wave, sometimes the flood wave is governed by the exogenous process, and during large floods, it is governed by the combination of the two.

The arrival of the flood wave through the Mamoré River together with the expansion of the flooded area downstream, depicted in Fig. 6a and b, is a strong indication that the flooding of the Llanos makes an important exogenous contribution to the initial phase of the flood, as suggested by Bourrel et al. (2009).

Although we observed in Fig. 6a that concomitant with the expansion of the flooding upstream, the flooded area also increased in isolated areas of the endogenous network, the contribution times to the Mamoré River of endogenous streams and lakes are likely to be much longer than the arrival of the flood wave through the Mamoré River. Therefore, in the initial phase, the flooding of the Llanos should occur mainly from the river main stem toward the floodplain.

To check for potential hydrodynamic effects in the exchange between the Mamoré main stem and the wetlands, we compared the water stages of the Mamoré River at Los Puentes and the Ibaré River, an endogenous tributary of the Mamoré River, at the Station of Puerto Almacén (Fig. 1) during the floods of 2007, 2008 and 2014. Because the two stations are relatively close, comparison of their water stage behavior provides an indication of the magnitude and direction of the river main-stem and floodplain exchange. Water stage was expressed in meters above sea level based on the altitude of the gauge's zero as estimated by Kosuth et al., (2006).

Fig. 8 indicates that, at the beginning of the rising limb of the flood, the water stage at the Mamoré River at Los Puentes was higher than in the Ibaré River at Puerto Almacén, suggesting that the direction of the flow was from the river to the floodplain. As the flood progressed, the water stage at the gauge station located at the wetlands was higher than the station in the Mamoré main-stem particularly during the 2008 and 2014 floods, indicating that the flow was from the wetlands toward the river. This process continues during the peak and for most of the recession of the flood wave. Finally, when the recession became more pronounced, differences in water level between the two stations gradually reduced and eventually inverted, suggesting a return to the initial conditions. Although the water stages during 2007 flood were similar in behavior, thus is, a steeper raise in Puerto Almacén gauge stations close to the peak-time, the water stages in this station remained only slightly higher than Los Puentes station and for a shorter time-period. This suggests that the flow from the wetlands toward the river was less important in magnitude and duration during 2007 compared to the other two events.

Our data confirm the hypothesis of Bourrel et al. (2009) with respect to the combination of exogenous and endogenous processes during large floods. In addition, the data suggest that, during major floods, the exogenous process is relatively short-lived and dominates only the first part of the rising phase. Because at peak time the difference in water stage between the wetlands and main stem is at its maximum (Fig. 8), lateral contribution from the wetlands to the river (endogenous process) appears to determine the magnitude and duration of the flooding. Moreover, the larger the flood, the more significant the flows from the wetlands towards the river: the 2014 flood produced the largest positive gradients from the wetlands to the river main stem and for a longer time-period, followed by the 2008 flood and finally the 2007 event. However, despite the

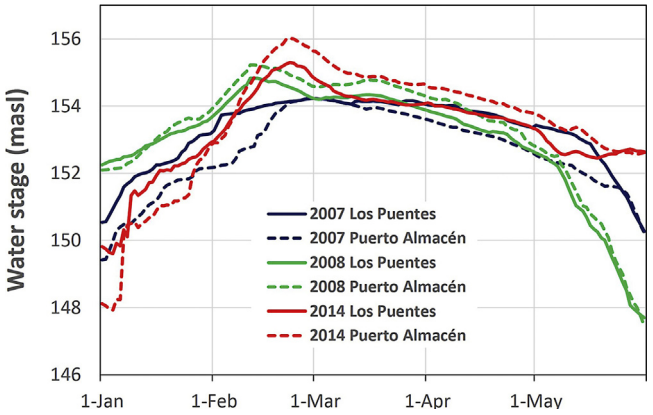

Fig. 8. Water stage at the station of the Mamoré River at Los Puentes (continuous lines) and the Ibaré River at Puerto Almacén (dotted lines) during the 2008 (green lines) and 2014 (red lines) floods. (For interpretation of the references to color in this figure legend, the reader is referred to the web version of this article.)

Table 2
Comparison between the wet season rainfall anomalies (in mm) during the three floods events for the floodplain (drainage areas with altitudes below 250 m) and for the piedmont and mountainous areas (drainage areas with altitude above 250 m) for the Mamoré River at Puerto Siles during the three flood events.

Period	Floodplain	Piedmonts and Mountains
Oct 2006–Mar 2007	48	−37
Oct 2007–Mar 2008	384	119
Oct 2013–Mar 2014	363	74

reduced duration of the exogenous phase, it is clear that it plays a crucial role in damping the flood by transferring water to the wetlands during the initial phase of the event.

Additional evidence about the relative importance of the local rainfall on the wetland areas compared to the exogenous processes during major floods is provided by Table 2, which shows rainfall anomalies of all three events for the Mamoré River at Puerto Siles Station for the period October–March. Based on Fig. 1, we arbitrary classified as floodplain the drainage area with altitude lower than 250 m, and as piedmonts and mountains the drainage area above 250 m of altitude. Although the analysis of accumulated values of rainfall anomalies have limitations since the magnitude of the hydrological response is closely related to intense rainfall events at daily to weekly time scales, rather than seasonal accumulated values, it is clear that rainfall anomalies where consistently higher in the floodplain in all events. In relative terms, accumulated rainfall anomalies in the floodplain were 85 mm, 265 mm and 289 mm higher in the floodplain compared to the piedmonts and mountains during the 2007, 2008 and 2014 events respectively.

5. Conclusions

Major flood events in the upper Madeira are characterized by the superposition of flood waves originating in the Beni-Madre de Dios River system (western upper Madeira) and the Mamoré–Guaporé river system (eastern upper Madeira). The concomitant peaks reaching the Madeira River at Abunã station, exacerbated by abundant local rainfall, result in higher peak discharges such as those observed during the 2007, 2008 and 2014 flood events. In the case of the 2007 event, the peak of the Madeira was enhanced due to a delay in the discharge of the Beni-Madre de Dios River system, which was in phase with the contribution of the Mamoré–Guajará system. During the 2008 flood, the peak of the Madeira River at Abunã resulted from the superposition of a late secondary peak from the Beni-Madre de Dios system with the peak of the Mamoré–Guaporé system, and it was augmented by intense local rainfall at Abunã station. Finally, in the 2014 flood, the flood wave from the Mamoré–Guaporé river system was faster and “in phase” with the contribution coming from the Beni-Madre de Dios river system. Because the discharges of the two river systems were the maximum recorded in the available series, the Madeira reached peak discharges never observed in the existing series.

In terms of flooded area, this study corroborated the estimations of Hamilton et al. (2004) in terms of the maximum flooded area. However, discrepancies were noted in terms of the mean flooded area, presumably due to differences in the methodology used for image processing.

The dynamics of the flooded area in the Llanos are strongly dependent on the timing and spatial distribution of positive rainfall anomalies. The magnitude of the flooding, on the other hand, is strongly dependent not only on the spatial distribution of the positive anomalies but also on the location of intense rainfall spots. This can be explained by the fact that flooded areas transform all rainfall into runoff, and therefore localized intense rainfall has an immediate and abrupt influence on river discharge. Obviously, this effect is more pronounced in the middle of the wet season, when the flooded area is enough large

that the hydrological response cannot be attenuated by soil water storage. In addition, the persistence of positive rainfall anomalies in March determines the duration of the flooding.

As suggested by Bourrel et al. (2009), floods in the Llanos are a combination of an exogenous process, which is a flood wave originating in the Mamoré upper drainage area; and an endogenous process, which is the contribution of the flooded area of the Llanos. Although the exogenous process appears to be important in the early phase of the flooding, dampening the incoming flood wave from the Andes piedmont, the endogenous process appears to be the most important in determining the magnitude and duration of the flooding of major floods.

Conflict of interest

None.

Acknowlegments

We thank the Hybam Project (Geodynamical, hydrological and biogeochemical control of erosion/alteration and material transport in the Amazon basin), the Servicio Nacional de Meteorologia e Hidrologia (SENAMHI) of Bolivia and Peru and the Agência Nacional de Águas (ANA- Brazil) for providing rainfall and streamflow data. We thank the Parapeti project (French Institute for Research and Development - IRD and Total Bolivia, Marc Pouilly) and the AMAZALERT Project (EU-FP7 Project 282644) for founding the acquisition of ALOS-PALSAR images. Thanks to Erwan Gensak, Laboratoire Geosciences Environnment Toulouse -GET and Sandro Klippel, Centro de Ciência do Sistema Terrestre CCST-INPE for their collaboration in the analysis of MODIS images. Finally, we specially thank the Coordenação de Aperfeiçoamento de Pessoal de Nível Superior CAPES and the Conselho Nacional de Desenvolvimento Científico e Tecnológico CNPq – Brazil.

Appendix A. Supplementary data

Supplementary data associated with this article can be found, in the online version, at http://dx.doi.org/10.1016/j.ejrh.2015.11.004.

References

Abril, G.I., et al., 2014. Amazon River carbon dioxide outgassing fuelled by wetlands. Nature 505 (7483), 395–398, http://dx.doi.org/10.1038/nature12797.
Alcantara, E.H., Stech, J., Novo, E., Shimabukuro, Y., Barbosa, C.C., 2008. Turbidity in the Amazon floodplain assessed through a spatial regression model applied to fraction images derived from MODIS/Terra. IEEE Trans. Geosci. Remote Sens., 2895–2905.
Alsdorf, D., Bates, P., Melack, J., Wilson, M., Dunne, T., 2007. Spatial and temporal complexity of the Amazon flood measured from space. Geophys. Res. Lett. 34 (8), L08402, http://dx.doi.org/10.1029/2007gl029447.
ANA, 2012. Orientações para consistência de dados pluviométricos. Superintendência de Gestão da Rede Hidrometeorológica, Brasilia.
Arnesen, A.S., et al., 2013. Monitoring flood extent in the lower Amazon River floodplain using ALOS/PALSAR ScanSAR images. Remote Sens. Environ. 130, 51–61, http://dx.doi.org/10.1016/j.rse.2012.10.035.
Arraut, E.M., Silva, T.S.F., Novo, E.M., 2013. Secas extremas na planicie de inundacao amazônica: alguns impactos sobre a ecologia e a biodiversidade. In: Borma, L.D.S., Nobre, C. (Eds.), Secas na Amazônia—causas e consequências. Oficina de textos, Sao Paulo.
Blaschke, T., 2010. Object based image analysis for remote sensing. ISPRS J. Photogramm. Remote Sens. 65 (1), 2–16, http://dx.doi.org/10.1016/j.isprsjprs.2009.06.004.
Bonnet, M.P., et al., 2008. Floodplain hydrology in an Amazon floodplain lake (Lago Grande de CuruaÃ). J. Hydrol. 349 (1â€“2), 18–30, http://dx.doi.org/10.1016/j.jhydrol.2007.10.055.
Bouchez, J. et al. 2012. Floodplains of large rivers: weathering reactors or simple silos? Chemical Geology, 332â€“333(0): 166–184. 10.1016/j.chemgeo.2012.09.032.
Bourrel, L., Phillips, L., Moreau, S., 2009. The dynamics of floods in the Bolivian Amazon Basin. Hydrol. Processes 23 (22), 3161–3167, http://dx.doi.org/10.1002/hyp.7384.
CEPAL, 2008. Evaluacion del Impacto Acumulado y Adicional Ocacionado por la Niña 2008 en Bolivia, Ministerio de Planificación del Desarrollo (MPD) de Bolivia, Secretaría Ejecutiva de la Comisión Económica para América Latina y el Caribe (CEPAL), La Paz-Bolivia.
Crespo, A., Van Damme, P.A., 2011. Spatial flood patterns in the Amazon Basin of Bolivia. In: Van Damme, P.A., Carvajal, F., Molina, J. (Eds.), Los Peces y Delfines de la Amazonia Boliviana: Hábitats, Potencialidades y Amenazas. Editorial Inia, Cochabamba - Bolivia, pp. 15–28.
Da Silva, J.S., et al., 2010. Water levels in the Amazon basin derived from the ERS 2 and ENVISAT radar altimetry missions. Remote Sens. Environ. 114 (10), 2160–2181, http://dx.doi.org/10.1016/j.rse.2010.04.020.
Da Silva, J.S., et al., 2012. Water level dynamics of Amazon wetlands at the watershed scale by satellite altimetry. Int. J. Remote Sens. 33 (11), 3323–3353.
de Lucia Lobo, F., Novo, E.M.L.M., Barbosa, C.C.F., Galvao, L.S., 2012. Reference spectra to classify Amazon water types. Int. J. Remote Sens. 33 (11), 3422–3442, http://dx.doi.org/10.1080/01431161.2011.627391.
Dunne, T., Mertes, L.A.K., Meade, R.H., Richey, J.E., Forsberg, B.R., 1998. Exchanges of sediment between the flood plain and channel of the Amazon River in Brazil. Geol. Soc. Am. Bull. 110 (4), 450–467, http://dx.doi.org/10.1130/0016-7606(1998)110<0450:EOSBTF>2.3.CO;2.
Espinoza, J.C., et al., 2014. The extremeflood in south-western Amazon basin: the role of tropical-subtropical South Atlantic SST gradient. Environ. Res. Lett. 9 (12), 124007.
Espinoza, J.C., et al., 2012. From drought to flooding: understanding the abrupt 2010–2011 hydrological annual cycle in the Amazonas River and tributaries. Environ. Res. Lett. 7 (2), 024008, http://dx.doi.org/10.1088/1748-9326/7/2/024008.
Espinoza Villar, J.C., et al., 2009. Spatio-temporal rainfall variability in the Amazon basin countries (Brazil, Peru, Bolivia, Colombia, and Ecuador). Int. J. Climatol. 29 (11), 1574–1594, http://dx.doi.org/10.1002/joc.1791.
Frappart, F.d.r., Calmant, S.p., Cauhopé, M., Seyler, F.d.r., Cazenave, A., 2006. Preliminary results of ENVISAT RA-2-derived water levels validation over the Amazon basin. Remote Sens. Environ. 100 (2), 252–264, http://dx.doi.org/10.1016/j.rse.2005.10.027.
Fundación-Milenio, 2014. Pérdidas economicas por inundaciones Enero—Febrero 2014, Informe Nacional de Coyuntura. Fundacion Milenio, La Paz.
Gloor, M., et al., 2013. Intensification of the Amazon hydrological cycle over the last two decades. Geophys. Res. Lett. 40 (9), 1729–1733, http://dx.doi.org/10.1002/grl.50377/full.

Guyot, J.L., 1993. Hydrogéochemie des Fleuves de l'amazonie Bolivienne. Universite de Bourdeaux, Bourdeaux.
Guyot, J.L., Fillzola, N., Quintanilla, J., Cortez, J., 1996. Dissolved solids and suspended sediment yields in the Rio Madeira basin, from the Bolivian Andes to the Amazon. In: Walling, D.E., Webb, B.W. (Eds.), Erosion and Sediment Yield: Global and Regional Perspectives. IAHS, Exeter, UK, pp. 55–64.
Hamilton, S.K., Sippel, S.J., Melack, J.M., 2002. Comparison of inundation patterns among major South American floodplains. J. Geophys. Res. Atmos. (1984–2012) 107 (D20), 5–14, http://dx.doi.org/10.1029/2000JD0000306, LBA 5-1-LBA.
Hamilton, S.K., Sippel, S.J., Melack, J.M., 2004. Seasonal inundation patterns in two large savanna floodplains of South America: the Llanos de Moxos (Bolivia) and the Llanos del Orinoco (Venezuela and Colombia). Hydrol. Processes 11, 2103–2116, http://dx.doi.org/10.1002/hyp.5559.
Hanagarth, W., 1993. Acerca de la geoecologia de las sabanas del Beni en el noreste de Bolivia. Instituto de Ecología, La Paz, Bolivia.
Hess, L., et al., 2015a. Wetlands of the Lowland Amazon Basin: extent, vegetative cover, and dual-season inundated area as mapped with JERS-1 Synthetic Aperture Radar. Wetlands 35 (4), 745–756, http://dx.doi.org/10.1007/s13157-015-0666-y.
Hess, L.L., et al., 2015b. LBA-ECO LC-07 Wetland Extent, Vegetation, and Inundation: Lowland Amazon Basin. ORNL DAAC, Oak Ridge, Tennessee, USA, http://dx.doi.org/10.3334/ORNLDAAC/1284.
Junk, W., 1997. General aspects of floodplain ecology with special reference to Amazonian Floodplains, The Central Amazon Floodplain. In: Ecological Studies. Springer, Berlin, Heidelberg, pp. 3–20, http://dx.doi.org/10.1007/978-3-662-03416-3_1.
Junk, W., 2013. Current state of knowledge regarding South America wetlands and their future under global climate change. Aquat. Sci. 75 (1), 113–131, http://dx.doi.org/10.1007/s00027-012-0253-8.
Junk, W., Worbes, M., 1997. The forest ecosystem of the floodplains, The Central Amazon Floodplain. In: Ecological Studies. Springer, Berlin, Heidelberg, pp. 223–265, http://dx.doi.org/10.1007/978-3-662-03416-3_11.
Junk, W.J., Bayley, P.B., Sparks, R.E., 1989. The flood pulse concept in river-floodplain systems. In: Dodge, D.P. (Ed.), Proceedings of the International Large River Symposium. Canadian Special Publication of Fisheries and Aquatic Sciences. Ontario, Canada, pp. 110–127.
Kayranli, B., Scholz, M., Mustafa, A., Hedmark, A., 2010. Carbon storage and fluxes within freshwater wetlands: a critical review. Wetlands 30 (1), 111–124, http://dx.doi.org/10.1007/s13157-009-0003-4.
Kosuth, P., Blitzkow, D., Cochonneau, G.R., 2006. Esta blishment of an Altimetric Reference Network over the Amazon Basin Using Satellite Radar Altimetry (Topex Poseidon). ESA Special Publication, pp. 68.
Lefevre, M., Remund, J., Albuisson, M., Wald, L., 2002. St Udy of Effective Distances for Interpolation Schemes in Meteorology, European Geophysical Society, 27th General Assembly. European Geophysical Society, pp. A-03429.
Marengo, J., Tomasella, J., Soares, W., Alves, L., Nobre, C., 2012. Extreme climatic events in the Amazon basin. Theor. Appl. Climatol. 107 (1–2), 73–85, http://dx.doi.org/10.1007/s00704-011-0465-1.
Marengo, J.A., et al., 2008. The drought of Amazonia in 2005. J. Clim. 21 (3), 495–516, http://dx.doi.org/10.1175/2007jcli1600.1.
Marengo, J.A., Soares, W.R., Saulo, C., Nicolini, M., 2004. Climatology of the low-level jet east of the andes as derived from the NCEP/NCAR reanalyses: characteristics and temporal variability. J. Clim. 17 (12), 2261–2280, http://dx.doi.org/10.1175/1520-0442(2004)017<2261:cotlje>2.0.co;2.
Marengo, J.A., Tomasella, J., Alves, L.M., Soares, W.R., Rodriguez, D.A., 2011. The drought of 2010 in the context of historical droughts in the Amazon region. Geophys. Res. Lett. 38 (12), L12703, http://dx.doi.org/10.1029/2011gl047436.
Martinez, J.-M., Le Toan, T., 2007. Mapping of flood dynamics and spatial distribution of vegetation in the Amazon floodplain using multitemporal SAR data. Remote Sens. Environ. 108 (3), 209–223, http://dx.doi.org/10.1016/j.rse.2006.11.012.
Meade, R.H., Dunne, T., Richey, J.E., Santos, U.d.M., Salati, E., 1985. Storage and remobilization of suspended sediment in the lower Amazon River of Brazil. Science 228 (4698), 488–490, http://dx.doi.org/10.1126/science.228.4698.488.
Melack, J.M., Forsberg, B., 2001. Biogeochemistry of Amazon floodplain lakes and associated wetlands. In: McClain, M.E., Victoria, R.L., Richey, J.E. (Eds.), Biogeochemistry of the Amazon Basin and its Role in a Changing World. Oxford Univ. Press, New York, pp. 235–276.
Melack, J.M., et al., 2004. Regionalization of methane emissions in the Amazon Basin with microwave remote sensing. Global Change Biol. 10 (5), 530–544, http://dx.doi.org/10.1111/j.1365-2486.2004.00763.x.
Mertes, L.A.K., et al., 1995. Spatial patterns of hydrology, geomorphology, and vegetation on the floodplain of the Amazon river in Brazil from a remote sensing perspective. Geomorphology 13 (1â€“4), 215–232, http://dx.doi.org/10.1016/0169-555X(95)00038-7.
Mertes, L.A.K., Dunne, T., Martinelli, L.A., 1996. Channel-floodplain geomorphology along the Solimões-Amazon River, Brazil. Geol. Soc. Am. Bull. 108 (9), 1089–1107, http://dx.doi.org/10.1130/0016-7606(1996)108<1089:cfgats>2.3.co;2.
Navarro, G., Maldonado, M., 2004. Geografía Ecológica de Bolivia, Vegetación y Ambientes Acuáticos. Editorial Centro de Ecología Difusión Simón I. Patiño, Santa Cruz, Bolivia.
Paiva, R.C.D., et al., 2013. Large-scale hydrologic and hydrodynamic modeling of the Amazon River basin. Water Resour. Res. 49 (3), 1226–1243, http://dx.doi.org/10.1002/wrcr.20067.
Phillips, O.L., et al., 2009. Drought sensitivity of the Amazon Rainforest. Science 323 (5919), 1344–1347, http://dx.doi.org/10.1126/science.1164033.
Plotzki, A., May, J.H., Veit, H., 2012. Review of past and recent fluvial dynamics in the Beni lowlands, NE Bolivia. Geogr. Helv. 66 (3), 164–172, http://dx.doi.org/10.5194/gh-66-164-2011.
Quegan, S., Le Toan, T., 1998. Analysing multitemporal SAR images. EUROPEAN SPACE AGENCY-PUBLICATIONS-ESA SP, 434: 17–28.
Quegan, S., Le Toan, T., Yu, J.J., Ribbes, F., Floury, N., 2000. Multitemporal ERS SAR analysis applied to forest mapping. IEEE Trans. Geosci. Remote Sens. 38 (2), 741–753.
Richey, J.E., Melack, J.M., Audenkampe, A.K., Ballester, V.M., Hess, L.L., 2002. Outgassing from Amazonian rivers and wetlands as a large tropical source of atmospheric CO2. Nature 416, 617–620, http://dx.doi.org/10.1038/416617a.
Roche, M.-A., Fernandez-Jauregui, C., 1988. Water resources, salinity and salt yields of the rivers of the Bolivian Amazon. J. Hydrol. 101 (1–4), 305–331, http://dx.doi.org/10.1016/0022-1694(88)90,042-x.
Roche, M.A., et al., 1992. Balance Hídrico Superficial de Bolivia. Orstom-Phicab.
Ronchail, J., et al., 2005. Inundations in the Mamore basin (south-western Amazon—Bolivia) and sea-surface temperature in the Pacific and Atlantic Oceans. J. Hydrol. 302 (1â€“4), 223–238, http://dx.doi.org/10.1016/j.jhydrol.2004.07.005.
Ronchail, J., et al., 2003. Hydrology and climate in the Southwestern Amazon Basin (Bolivia). Geophys. Res. Abstr. 5 (10982).
Rudorff, C.M., Galvao, L.S., Novo, E.M.L.M., 2009. Reflectance of floodplain waterbodies using EO-1Hyperion data from high and receding flood periods of the Amazon River. Int. J. Remote Sens. 30 (10), 2713–2720, http://dx.doi.org/10.1080/01431160902755320.
Rudorff, C.M., Melack, J.M., Bates, P.D., 2014. Flooding dynamics on the lower Amazon floodplain: 2. Seasonal and interannual hydrological variability. Water Resour. Res. 50 (1), 635–649, http://dx.doi.org/10.1002/2013wr014714.
Siqueira-Júnior, J.L.S., Tomasella, J., Rodriguez, D.A., 2015. Impacts of future climatic and land cover changes on the hydrological regime of the Madeira River basin. Clim. Change 129 (1–2), 117–129, http://dx.doi.org/10.1007/s10584-015-1338-x.
Tomasella, J., et al., 2010. The droughts of 1996-1997 and 2004-2005 in Amazonia: hydrological response in the river main-stem. Hydrol. Processes 25 (8), 1228–1242, http://dx.doi.org/10.1002/hyp.7889.
Tomasella, J., et al., 2013. The droughts of 1997 and 2005 in Amazonia: floodplain hydrology and its potential ecological and human impacts. Clim. Change 116 (3–4), 723–746.
Trimble, 2011. eCognition Developer 8.7 - Reference Book, München, Germany.
Viers, J.r.m., et al., 2005. The influence of the Amazonian floodplain ecosystems on the trace element dynamics of the Amazon River mainstem (Brazil). Sci. Total Environ. 339, 219–232, http://dx.doi.org/10.1016/j.scitotenv.2004.07.034.
Woodhouse, I.H., 2006. Introduction to microwave remote sensing. CRC press.